

Non-Abelian Majorana modes protected by an emergent second Chern number

Cheung Chan and Xiong-Jun Liu*

International Center for Quantum Materials, School of Physics, Peking University, Beijing, 100871, China and Collaborative Innovation Center of Quantum Matter, Beijing 100871, China

The search for topological superconductors and non-Abelian Majorana modes ranks among the most fascinating topics in condensed matter physics. There now exist several fundamental superconducting phases which host symmetry protected or chiral Majorana modes. The latter, namely the chiral Majorana modes are protected by Chern numbers in even dimensions. Here we propose to observe novel chiral Majorana modes by realizing Fulde-Ferrell-Larkin-Ovchinnikov state, i.e. the pairing density wave (PDW) phase in a Weyl semimetal which breaks time-reversal symmetry. Without symmetry protection, the 3D gapped PDW phase is topologically trivial. However, a vortex line generated in such phase can host chiral Majorana modes, which are shown to be protected by an emergent second Chern number of a synthetic 4D space generalized from the PDW phase. We further show that these chiral modes in the vortex rings obey 3D non-Abelian loop-braiding statistics, which can be applied to topological quantum computation.

Eighty years ago, Ettore Majorana proposed a new fermion which is identical to its antiparticle and now called Majorana fermion (MF) [1], and speculated that it might interpret neutrinos. While the evidence of MFs as elementary particles in high energy physics is yet elusive, the search for MFs has energetically revived in condensed matter physics and become an exciting pursuit in recent years [2–4]. Rather than being elementary particles, MFs can emerge as quasiparticles localized in surfaces or defects of p -wave topological superconductors (SCs) [5, 6]. Besides the early proposed intrinsic p -wave SCs, the studies have shown that combining conventional s -wave SC and spin-orbit (SO) coupled systems can render effective p -wave pairing states [7–11], bringing the realization of MFs to realistic solid state experiments. In the last couple of years, the suggestive signatures of Majorana modes have been observed with heterostructures formed by s -wave SCs and semiconductor nanowires [12–14], magnetic chains [15], or topological insulators [16, 17].

MFs in different dimensional SCs exhibit fundamentally distinct properties. In odd dimensions topological SCs classified by integers necessitate symmetry protection, such as time-reversal (TR) and particle-hole symmetries, so do Majorana modes in such systems. The famous examples include the 1D Kitaev chain [18] which belongs to BDI symmetry class, with Majorana zero modes at chain ends being protected by chiral symmetry, and the 3D TR invariant (class DIII) topological SC [19–22] which hosts helical Majorana surface modes protected by TR symmetry and characterized by a 3D winding number. In contrast, topological SCs in even dimensions can be chiral topological orders which require no symmetry protection. A notable toy model is the 2D $p + ip$ SC [5, 23] which is a non-Abelian chiral topological order classified by the 1st Chern number, and hosts chiral Majorana edge modes whose gapping is forbidden by energy conservation. Stacking $p + ip$ SCs along the third direction yields a 3D system [24] with anisotropic Majorana surface modes corresponding to, however, the

Chern numbers of the original 2D subspace rather than any 3D topological invariant, implying that these surface modes are not intrinsic chiral states of the 3D phase. As a consequence, the stacked phase is not a 3D non-Abelian topological order, unlike the 2D $p + ip$ chiral phases.

Here we propose to observe novel chiral Majorana modes by realizing Fulde-Ferrell-Larkin-Ovchinnikov state [25, 26], i.e. pairing density wave (PDW) phase in a 3D Weyl semimetal whose study attracted great interests only recently [27–33], and show that such modes can realize exotic non-Abelian loop braiding statistics, applicable to topological quantum computation [34–36]. While the 3D gapped PDW phase is topologically trivial, a vortex line generated in this phase can host intrinsic chiral MFs which are protected by an emergent 2nd Chern number of a synthetic 4D space generalized from the physical 3D system. This study shows that the gapped PDW phase, being trivial in 3D, is an emergent non-Abelian topological order in a 4D synthetic space.

Model.—We start with a minimal model for Weyl semimetal tuned by SO coupling, which can be realized for cold atoms based on a recent experiment [37, 38], together with an attractive Hubbard interaction of strength U which can drive superconducting/superfluid phases. The present Weyl-Hubbard model is described by

$$H = \sum_{\mathbf{p}} \psi_{\mathbf{p}}^{\dagger} h_{\mathbf{p}} \psi_{\mathbf{p}} - U \sum_{\mathbf{i}} n_{\mathbf{i}\uparrow} n_{\mathbf{i}\downarrow}, \quad (1)$$

$$h_{\mathbf{p}} = [m_z - 2t_0(\cos p_x + \cos p_y) - 2t_z^c \cos p_z] \sigma_z + 2t_{\text{SO}}(\sin p_x \sigma_x + \sin p_y \sigma_y) - \mu - 2t_z^s \sin p_z,$$

where the spinor $\psi_{\mathbf{p}} = (c_{\mathbf{p}\uparrow}, c_{\mathbf{p}\downarrow})$, the particle number operator $n_{\mathbf{i}\sigma} = c_{\mathbf{i}\sigma}^{\dagger} c_{\mathbf{i}\sigma}$, t_0 (t_{SO}) is the coefficient of spin-conserved (spin-flipped) hopping in x - y plane, $\sigma_{x,y,z}$ are Pauli matrices on spin space, and μ is chemical potential. Moreover, we consider the hopping terms along z direction with $(t_z^c, t_z^s) = t_z(\cos \varphi_0, \sin \varphi_0)$, which break inversion symmetry of the Weyl semimetal unless $\varphi_0 = n\pi/2$ with integer n . For $m_z = 4t_0 + 2t_z^c \cos Q$ ($0 < Q < \pi$),

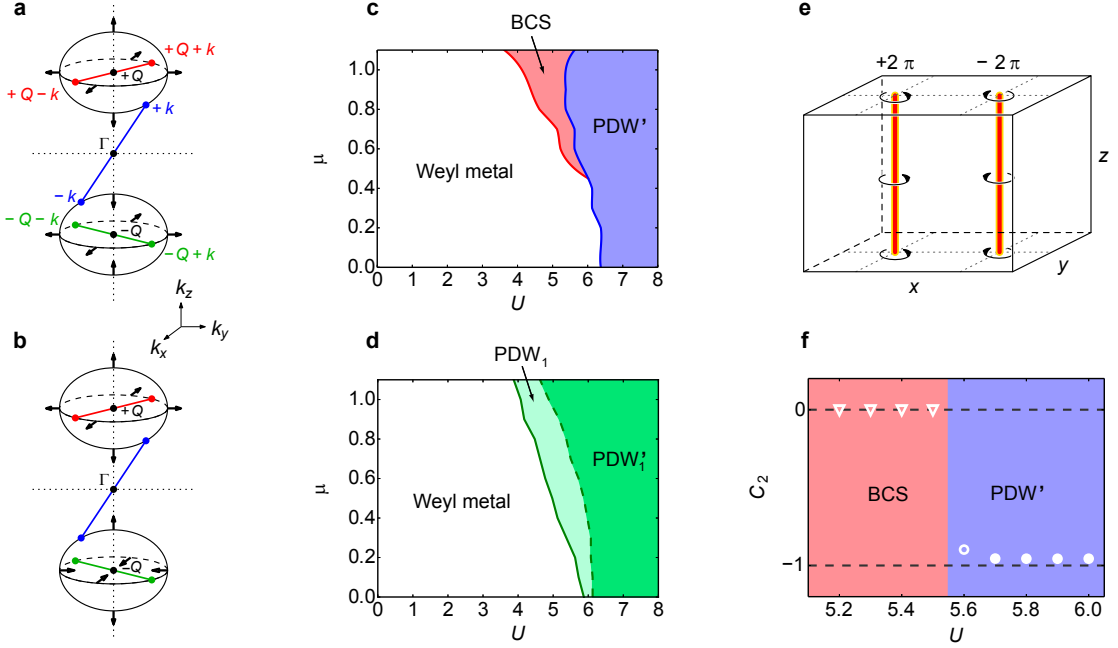


FIG. 1: Weyl metals, mean field phase diagrams, vortex line configuration, and 2nd Chern numbers. (a,b) Schematic for Fermi surfaces and superconducting pairing of inversion symmetric (for a) and inversion symmetry broken (for b) Weyl metals. The two ellipsoids centered at \mathbf{Q}_{\pm} are the Fermi surfaces. The spin orientations, shown by black arrows, at the Fermi surface around \mathbf{Q}_{-} is flipped when $0 < \mu < 2t_z^s \sin |Q_{\pm}|$. The colored lines represent the pairing order parameters $\Delta_{\mathbf{q}}$ with $\mathbf{q} = 0, 2\mathbf{Q}_{\pm}$. (c,d) Phase diagram for inversion symmetric (for c) and inversion symmetry broken (for d) Weyl metal versus attractive Hubbard interaction U and chemical potential μ . (e) Configuration of two vortex lines with opposite vorticities. (f) The emergent 2nd Chern number C_2 for a 4D synthetic space generalized from the 3D physical system in the inversion symmetric case and with $\mu = 0.7$. Upon increasing U , the system undergoes a transition from BCS to PDW' phase. The circles (triangles) gives the 2nd Chern number in BCS (PDW') phase, which shows $C_2 \approx -0.956$ for PDW' phase.

the Weyl semimetal has two nodal points of chiralities $\chi = \pm$ located at $\mathbf{Q}_{\chi} = (0, 0, \chi Q)$ and with energies $E_{\pm} = -\mu \mp 2t_z^s \sin Q$, respectively. Without loss of generality, in the following we shall choose $Q = \frac{2\pi}{3}$ and $t_{0,z} = t_{SO} = 1.0$ to facilitate further discussion.

The superconducting/superfluid phases can be induced with an attractive interaction $U > 0$. The possible pairing orders are of two distinct types, namely the s -wave BCS and PDW phases, as sketched in Fig. 1(a). The former describes a uniform pairing order Δ_0 occurring between two different Weyl cones and with zero center-of-mass momentum of Cooper pairs, while the latter are spatially modulated orders $\Delta_{2\mathbf{Q}_{\pm}}$ occurring within each Weyl cone and the Cooper pairs have nonzero center-of-mass momentum [33, 39–42]. These pairing orders can be written as $\Delta_{\mathbf{q}} = \frac{U}{2N} \sum_{\mathbf{k}} \langle c_{\mathbf{q}/2+\mathbf{k}\uparrow} c_{\mathbf{q}/2-\mathbf{k}\downarrow} \rangle$, with $\mathbf{q} = 0, 2\mathbf{Q}_{\pm}$, and N being number of sites, and the interaction is decoupled into $\mathcal{H}_{MF} = \sum_{\mathbf{k}, \mathbf{q}} \Delta_{\mathbf{q}} c_{\mathbf{q}/2+\mathbf{k}\uparrow}^{\dagger} c_{\mathbf{q}/2-\mathbf{k}\downarrow}^{\dagger} + \text{h.c.}$ Here \mathbf{k} is summed over the entire Brillouin zone. Having both BCS and PDW phases, the order parameter takes the following generic form in real space

$$\Delta(\mathbf{r}) = \Delta_0 + \Delta_{+2Q} e^{i2\mathbf{Q} \cdot \mathbf{r}} + \Delta_{-2Q} e^{i2\mathbf{Q}' \cdot \mathbf{r}}. \quad (2)$$

The BCS and PDW orders may compete governed by

following underlying mechanisms [43]. The BCS pairing connects two different Weyl cones with opposite chiralities and cannot fully gap out the bulk, since the chiralities, characterizing the topology of the Weyl Fermi surfaces, cannot be adiabatically connected without closing the bulk gap. Accordingly, the BCS phase renders a Weyl SC with four nodal points [39]. In contrast, the PDW order can fully gap out the bulk since the pairings do not connect the two Weyl cones but fold up the original Brillouin zone due to its spatial modulation. Nevertheless, such spatial modulation may cost extra energy. Below we perform a self-consistent study of the complete phase diagram in different regimes.

The numerical simulation reveals different phase diagrams versus μ and U for the inversion-symmetric [Fig. 1(b)] and inversion symmetry broken [Fig. 1(d)] Weyl metals. For the inversion-symmetric Weyl metal given by $\varphi_0 = 0$, a direct transition from the Weyl metal phase to the PDW' phase, which has $|\Delta_{+2Q}| = |\Delta_{-2Q}| \gg |\Delta_0| \neq 0$, is obtained by increasing U in the low chemical potential regime with $|\mu| < \mu_c$ and $\mu_c \sim 0.4$. The equality $|\Delta_{+2Q}| = |\Delta_{-2Q}|$ in the PDW' phase is a consequence of the inversion symmetry. However, when μ is tuned away from Weyl point and beyond the critical value

$|\mu| > \mu_c$, the BCS phase with $\Delta_0 \neq 0$ and $\Delta_{\pm 2Q} = 0$ appears between the Weyl metal and PDW' phase. This result reflects that the pairings within each Weyl Fermi surface dominates over those between two different Weyl pockets in relatively low chemical potential regime. On the other hand, if the inversion symmetry is broken, the BCS phase is suppressed, and the system enters from Weyl metal into PDW₁ state first and then PDW'₁ phase by increasing U , as shown in Fig. 1(d) with $\varphi_0 = \frac{3}{32}\pi$. The PDW₁ phase is characterized by $|\Delta_{+2Q}| \geq |\Delta_{-2Q}|$ for $\mu \geq 0$ and $\Delta_0 = 0$, while in the PDW'₁ phase a small BCS order $|\Delta_0| < |\Delta_{\pm 2Q}|$ also emerges.

Vortex Line Modes.—Both BCS and PDW states have only the particle-hole symmetry, so they are class D SCs according to the Altland-Zirnbauer symmetry classification [44]. From the current topological classification theory [20–22], both BCS and PDW phases are $p_x + ip_y$ SCs stacked along z direction. Nevertheless, the two phases exhibit fundamental distinction in the excitations along vortex lines generated to the pairing orders.

We consider first the vortex line excitations for the PDW dominated phase. For simplicity, we take that $|\Delta_{+2Q}| = |\Delta_{-2Q}|$ and $\Delta_0 = 0$, since a small perturbative BCS order does not affect the results. Let a vortex line with winding number n be along z -axis and attached to Δ_{+2Q} , so that $\Delta_{+2Q} = |\Delta_{+2Q}| \exp[in\phi(\mathbf{r})]$, where the azimuthal angle $\tan(\phi) = y/x$. In the low energy limit we can write down the effective Hamiltonian by linearizing the 3D Weyl cone Hamiltonian around \mathbf{Q}_+ point

$$H_{\text{eff}} = - \left(\sum_{j=x,y,z} iv_j \sigma_j \partial_j + \mu_{\text{eff}} \right) \tau_z + \bar{\Delta}(\rho) \cos(n\phi) \tau_x + \bar{\Delta}(\rho) \sin(n\phi) \tau_y, \quad (3)$$

where v_j is the Fermi velocity along j -th direction, μ_{eff} is the chemical potential measured from the Weyl node, and τ 's are Pauli matrices for the Nambu space spanned by $\hat{f}(\mathbf{r}) = [c_{\uparrow}(\mathbf{r}), c_{\downarrow}(\mathbf{r}), c_{\uparrow}^{\dagger}(\mathbf{r}), -c_{\downarrow}^{\dagger}(\mathbf{r})]^T$. We implicitly assumed that the vortex line is located at the origin in the (x, y) -plane along z -axis, hence we choose cylindrical coordinate (ρ, ϕ, z) . Here $\bar{\Delta}$ is a function that $\bar{\Delta}(\rho \rightarrow 0) = 0$ and $\bar{\Delta}(\rho \rightarrow \infty) = \text{constant}$ and $n\phi$ is the phase winding of the PDW component. As detailed in the Supplementary Material [43], for $n = \pm 1$ the Majorana in-gap modes can be obtained analytically and satisfy $H_{\text{eff}} \gamma_z(\rho, \phi, k_z) = \mathcal{E}_{k_z} \gamma_z(\rho, \phi, k_z)$, with eigenvalues $\mathcal{E}_{k_z} = \text{sgn}(n) \text{sgn}(v_x v_y) v_z k_z$, which implies that the vortex Majorana modes are chiral. The Majorana operator can be constructed by $\hat{\gamma}_z(k_z) = \int d^2 \mathbf{r} \gamma_z(\rho, \phi, k_z) \hat{f}(\rho, \phi, k_z)$, with $\hat{\gamma}_z(k_z) = \hat{\gamma}_z^{\dagger}(-k_z)$ for real MFs. It can be seen that the chirality $\chi_{\text{M}\ell} = \text{sgn}(n v_x v_y v_z)$ of the vortex Majorana modes related to the vortex winding n and Weyl node chirality χ . With the chiral properties of Majorana modes the above solution can be generalized to the case with a generic winding number $n = \mathcal{N}$. Actually, such a vortex line is topologically equivalent to $|\mathcal{N}|$ vortex lines

with unity winding $n = \text{sgn}(\mathcal{N})$. In the later case each vortex line hosts a branch of chiral Majorana modes. Due to the chiral property putting the n branches of vortex modes together cannot annihilate them, yielding n chiral Majorana vortex modes. Nevertheless, in the continuous limit a Majorana zero mode is obtained at $k_z = 0$ only when n is an odd integer.

The chirality of Majorana vortex modes imply that these modes are gapless and traverse the bulk gap of the PDW phase. To confirm this result, we perform a full real-space numerical calculation of the Majorana modes based on the lattice model. In particular, we consider the inversion symmetric Weyl metal with $\mu = 0.7$ and $U = 5.8$. The self-consistent calculation reveals a PDW' phase with $\Delta_{\pm 2Q} \approx 0.201$ and $\Delta_0 \approx -1.85 \times 10^{-2}$, and the system has a bulk gap $E_{\text{gap}} \approx 0.21$. We consider a vortex line ($n = 1$) and anti-vortex line ($n = -1$) along z -axis, separated from each other in x - y plane, and attached to one of $\Delta_{0, \pm 2Q}$, as sketched in Fig. 1(e). With this configuration appropriate periodic boundary condition can be applied in the numerical calculation. The local spectral function $A(x, y, k_z, E)$ can be obtained from the retarded Green's function $G^R(E)$ of the system

$$A = -\frac{1}{\pi} \sum_{s=\uparrow, \downarrow} \Im \langle x, y, k_z, s | G^R(E) | x, y, k_z, s \rangle, \quad (4)$$

where $|x, y, k_z, s\rangle$ is the Bloch basis with momentum k_z and in real space for x - y plane [43]. Computing $A(k_z, E)$ near the vortex core gives the energy spectra of the bulk and the corresponding vortex lines.

Fig. 2(a) and (b) show the spectra measured from the vortex line ($n = 1$) and anti-vortex line ($n = -1$), respectively. It is clear that in both cases the chiral Majorana vortex modes traverse the bulk gap connecting the lower and upper bands. The chirality of these modes depends on the vortex line winding number, consistent with the previous analytic solution. This result is fundamentally different from that for a BCS dominated phase, as shown in Fig. 2(c), where we compute the Majorana modes by attaching vortex and anti-vortex lines to Δ_0 with $\Delta_0 = 0.25$ and $\Delta_{\pm 2Q} = 0$. Majorana zero-energy flat bands associated with the vortex lines are obtained. These Majorana zero modes are simply the vortex modes of $p_x + ip_y$ SCs with different momenta k_z .

Emergent 2nd Chern number.—Chiral gapless modes have to be protected by chiral topological invariants, e.g. the Chern numbers. However, it can be verified that for any 2D sub-plane incorporating z -axis the 1st Chern number of the PDW phase is zero. Moreover, the 3D system is also topologically trivial [20, 21] without symmetry protection. As a result, a higher Chern number [24, 45, 46] may protect the Majorana vortex line modes. Note that the SC order can be parameterized by its phase factor $\Delta_{\mathbf{q}} e^{in\theta}$, where $\theta \in [0, 2\pi)$ forms a 1D periodic parameter space S^1 . Together with the 3D lattice,

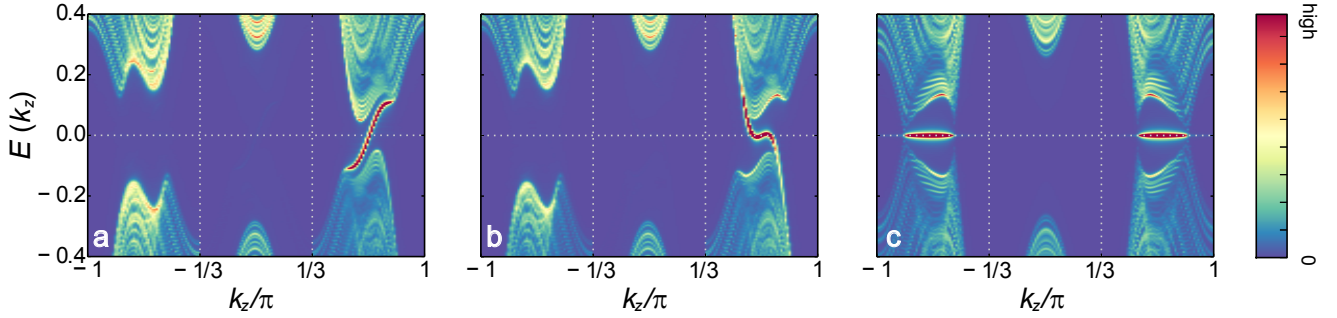


FIG. 2: Chiral Majorana modes as in-gap bound states to a vortex line. (a-b) Spectral functions $A(k_z, E)$ in the inversion symmetric Weyl metal with PDW orders obtained from self consistent mean field for $\mu = 0.7$ and $U = 5.8$. The vortex line is attached to Δ_{+2Q} , with winding number $n = +1$ for (a) and $n = -1$ for (b). (c) Spectral function $A(k_z, E)$ for the BCS dominated phase in the inversion symmetric Weyl metal with $\Delta_0 = 0.25$. Two segments of Majorana flat bands are obtained.

we construct a 4D synthetic space $T^4 = T^3 \times S^1$ spanned by $\mathbf{p} = (\mathbf{p}, p_\theta)$ with $\mathbf{p} = (p_x, p_y, p_z)$ and $p_\theta = \theta$. In this synthetic 4D space we define the 2nd Chern number by

$$C_2 = \frac{1}{32\pi^2} \int_{T^4} d^4\mathbf{p} \epsilon_{ijkl} \text{Tr}[\mathbf{F}_{ij}\mathbf{F}_{kl}] \in \mathbb{Z}, \quad (5)$$

where ϵ is the antisymmetric tensor and \mathbf{F}_{ij} are the gauge field strengths calculated from the eigenvectors of the parameterized mean-field Hamiltonian $H(\mathbf{p}, p_\theta)$. We calculate the 2nd Chern number for BCS dominated and PDW phases, as shown numerically in Fig. 1(f). It is found that $C_2 = 0$ for the BCS dominated phase, while $C_2 \approx -0.956$ for the PDW phase obtained with the same parameters except for U as in Fig. 2(a). The deviation of C_2 from an integer is due to finite size effect [43].

The difference in the 2nd Chern number C_2 uncovers the essential distinction between the BCS and PDW phases realized in a Weyl semimetal. The BCS phase is a reminiscent of 3D quantum Hall effect which hosts chiral edge states and dislocation line modes, while these modes are all essentially protected by 1st Chern number, rather than 2nd Chern number, in 2D sub-planes [24]. In contrast, the protection of chiral Majorana vortex modes by the emergent 2nd Chern number shows that the gapped PDW phase, while being trivial in the 3D, *is an intrinsic topological order in the 4D synthetic space*.

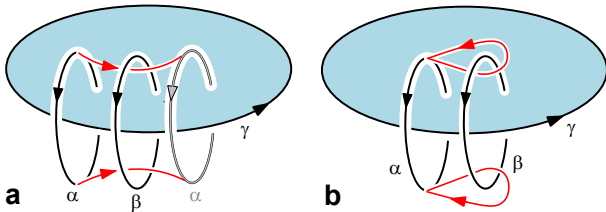


FIG. 3: Three-loop braiding of chiral Majorana modes. (a) Self braiding of the loops α and β , pierced by the third loop γ . (b) Full braiding of loops α and β .

Non-Abelian loop braiding statistics.—Interpreting the

gapped PDW phase as an intrinsic topological order in the 4D synthetic space is of high nontriviality. An important consequence is that the chiral Majorana modes may obey new type non-Abelian statistics, for which we consider vortex rings with winding number $n = 1$ and perform a three-loop braiding [47] as sketched in Fig. 3. From the particle-hole symmetry and chirality of the Majorana spectrum of a vortex ring, which is threaded by even or odd number of vortex lines, is generically given by $E_l = (l + 1/2)\mathcal{E}_0(L)$ or $E_l = l\mathcal{E}_0(L)$, where l is integer and $\mathcal{E}_0(L)$ depends on the vortex ring size L . A vortex ring in the former case contains even number of chiral Majorana modes without zero energy state, while in the later case each vortex ring harbors odd number of modes including a Majorana zero mode, which is essential for the realization of non-Abelian loop braiding statistics.

From the above result we know that the vortex rings α and β in Fig. 3, which are linked to γ separately, host one Majorana zero mode in each ring, while the vortex ring γ , which has an even linking number, harbors no zero mode. In this case, let ψ_j ($j = \alpha, \beta, \gamma$) denote the j -th vortex ring state which includes all chiral Majorana modes. Under a full three-loop braiding between α and β , pierced by γ [Fig. 3(b)], we can show that $\psi_\alpha, \psi_\beta \rightarrow -\psi_\alpha, -\psi_\beta$, while ψ_γ is unchanged. A single braiding is then followed by $\psi_\alpha \rightarrow \psi_\beta$ and $\psi_\beta \rightarrow -\psi_\alpha$ [Fig. 3(a)], which shows the braiding operator to be $\mathcal{B}_{\alpha\beta}(\gamma) = \exp(\frac{\pi}{4}\psi_\alpha\psi_\beta)$ [23], giving 3D non-Abelian loop braiding statistics. We note that taking different vortex ring configurations may bring rich different non-Abelian loop braiding statistics.

In conclusion, we have uncovered an emergent 4D non-Abelian topological order based on a superconducting Weyl semimetal, which hosts chiral Majorana modes protected by the 2nd Chern number. This topological phase is distinct from the known topological superconductors in the 1D to 3D systems, and is beyond the ten-fold Altland-Zirnbauer symmetry classification (Discussion in [43]). Thus our results may show insight into the search for new

non-Abelian topological states. Moreover, the present result reveals a real physical system to explore the exotic 3D non-Abelian loop-braiding statistics, and shall push forward the studies in both theory and experiment based on realistic solid state materials and cold atom platforms.

We thank Frank Wilczek and Z. D. Wang for valuable discussions. This work is supported by MOST (Grant No. 2016YFA0301604), NSFC (No. 11574008), and Thousand-Young-Talent Program of China.

Supplemental Material Non-Abelian Majorana modes protected by an emergent second Chern number

I. Self-consistent mean field study

A. Brillouin zone folding

The Weyl-Hubbard model can be solved self-consistently by introducing both the BCS and PDW pairing orders. The mean field Hamiltonian is given by

$$H_{\text{MF}} = \sum_{\mathbf{p}} \psi_{\mathbf{p}}^{\dagger} h_{\mathbf{p}} \psi_{\mathbf{p}} + \mathcal{H}_{\text{MF}} \quad (\text{S1})$$

$$h_{\mathbf{p}} = [m_z - 2t_0(\cos p_x + \cos p_y) - 2t_z^c \cos p_z] \sigma_z + 2t_{\text{SO}}(\sin p_x \sigma_x + \sin p_y \sigma_y) - \mu - 2t_z^s \sin p_z \quad (\text{S2})$$

$$\mathcal{H}_{\text{MF}} = \sum_{\mathbf{k}, \mathbf{q}} \Delta_{\mathbf{q}} c_{\mathbf{q}/2+\mathbf{k}\uparrow}^{\dagger} c_{\mathbf{q}/2-\mathbf{k}\downarrow}^{\dagger} + \text{h.c.} \quad (\text{S3})$$

$$\Delta_{\mathbf{q}} = \frac{U}{2N} \sum_{\mathbf{k}} \langle c_{\mathbf{q}/2+\mathbf{k}\uparrow} c_{\mathbf{q}/2-\mathbf{k}\downarrow} \rangle, \quad (\text{S4})$$

where the Hubbard interaction is attractive for $U > 0$, and the parameter φ_0 governs the inversion symmetry of the system, with $t_z^s = t_z \sin \varphi_0$, $t_z^c = t_z \cos \varphi_0$, $m_z = 4t_0 + 2t_z^c \cos Q$, and the spinor operator $\psi_{\mathbf{p}} = (c_{\mathbf{p}\uparrow}, c_{\mathbf{p}\downarrow})$. The BCS order corresponds to $\mathbf{q} = 0$ and PDW order corresponds to $\mathbf{q} = 2\mathbf{Q}_{\pm}$, with $\mathbf{Q}_{\pm} = \pm Q \hat{e}_z$. The PDW order breaks the translational symmetry by connecting two Bloch states (one particle and one hole) with momenta \mathbf{k} and $-\mathbf{k} + 2Q\hat{e}_z$, respectively. An importance consequence is that the original Brillouin zone (BZ) folds up into $2\pi/Q$ sub-Brillouin zones if Q is a commensurate momentum.

For convenience we choose here $Q = 2\pi/3$ and $t_{0,z} = t_{\text{SO}} = 1$ for the present study. The different choice of Q will not qualitatively change the present results. With the PDW order the reduced BZ is $1/3$ of the original BZ. The Hamiltonian can then be written in the form

$$H_{\text{MF}} = \frac{1}{2} \sum_k \tilde{\psi}_k^{\dagger} \mathcal{H}_{Q,k} \tilde{\psi}_k, \quad \mathcal{H}_{Q,k} = \begin{bmatrix} h_{Q,k} & \hat{\Delta} \\ \hat{\Delta}^{\dagger} & -h_{Q,-k}^T \end{bmatrix} \quad (\text{S5})$$

where we take the reduced BZ as $k_{x,y} \in [-\pi, \pi)$ and $k_z \in [-\pi/3, \pi/3)$, and denote basis for the reduced BZ by

$$\tilde{\psi}_k^T = \left(c_{Q+k\uparrow}, c_{k\uparrow}, c_{-Q+k\uparrow}, (\uparrow \rightarrow \downarrow); c_{Q-k\uparrow}^{\dagger}, c_{-k\uparrow}^{\dagger}, c_{-Q-k\uparrow}^{\dagger}, (\uparrow \rightarrow \downarrow) \right).$$

The explicit form of $h_{Q,k}$ is obtained by restricting the momentum of the Bloch Hamiltonian $h_{\mathbf{p}}$ within a sub-BZ. The order parameter $\hat{\Delta}$ in the matrix form reads

$$\hat{\Delta} = \begin{bmatrix} & \Delta_{[Q]} \\ -\Delta_{[Q]} & \end{bmatrix}, \quad \Delta_{[Q]} = \begin{bmatrix} \Delta_{+2Q} & \Delta_{-2Q} & \Delta_0 \\ \Delta_{-2Q} & \Delta_0 & \Delta_{+2Q} \\ \Delta_0 & \Delta_{+2Q} & \Delta_{-2Q} \end{bmatrix}. \quad (\text{S6})$$

We note that this system with reduced translational symmetry obeys a particle-hole symmetry defined as

$$\tau_x \mathcal{H}_{Q,k} \tau_x = -\mathcal{H}_{Q,-k}^T,$$

implying that the states at (k, E) and $(-k, -E)$ in the reduced BZ, instead of the unfolded BZ, form a particle-hole pair. Here τ_x is the Pauli matrix acting on the Nambu space.

B. Mean field phase diagram

Utilizing Eqs. (S1) to (S4), we can iteratively compute the eigenvectors of the Hamiltonian and hence $\Delta_{\mathbf{q}}$'s until convergence. The resulting mean field phase diagrams against attractive interaction strength U and chemical potential μ are shown in Figs. 1(c) and (d) in the main text for the inversion symmetric ($\varphi_0 = 0$) and inversion symmetry broken ($\varphi_0 = \frac{3}{32}\pi$) Weyl metals respectively. Since the phase diagrams are symmetric with respect to $\mu \rightarrow -\mu$ due to a ‘‘particle-hole symmetry’’ that the Hamiltonian (S1) possesses, so only the results for $\mu \geq 0$ is presented. We also restrict ourselves to $\mu < 1$ such that the systems resemble a Weyl metal and hence the choice $\varphi_0 = \frac{3}{32}\pi$ for the inversion symmetry broken Weyl metal. For $\mu \gtrsim 1$, the systems are always gapless regardless of the presence of BCS or PDW orders and hence no well-defined gapped topological state for defect modes.

The mean field phase diagrams show that the presence of superconducting orders require a finite U . For small μ , this can be understood in terms of the vanishing density of states near the Fermi energy. Moreover, the non-ideal nesting of Fermi surfaces is another reason for the presence of orders only with finite U [41]. This is in sharp contrast with the mean field analysis using Weyl nodes with ideal nesting condition [39]. One can indeed improve the superconducting nesting by choosing, e.g., $Q = \pi/2$ (actually ideal nesting in this case). However, in the case of $Q = \pi/2$, either one of $\Delta_{\pm 2Q}$ can already gap out the whole system. Attaching vortex line to one PDW order would induce two chiral Majorana modes of opposite chiralities separately at two Weyl nodes, and hence a null second Chern number. This is undesirable for the study of the chiral Majorana modes that are nonetheless the main focus of the paper.

II. Analytic results of Majorana modes in the low energy limit

In this section, we analytically derive the vortex line chiral Majorana modes in a low energy effective Hamiltonian for a single node in the Weyl metal with pairing of one PDW component. Consider the effective Hamiltonian

$$H_{\text{eff}} = - \left(\sum_{j=x,y,z} iv_j \sigma_j \partial_j + \mu_{\text{eff}} \tau_z + \bar{\Delta}(r) \cos(n\phi) \tau_x + \bar{\Delta}(r) \sin(n\phi) \tau_y \right), \quad (\text{S7})$$

where μ_{eff} is the effective chemical potential away from the Weyl node and τ 's (σ 's) are the Pauli matrices for the Nambu (spin) space spanned by $f^T(\mathbf{r}) = [c_{\uparrow}(\mathbf{r}), c_{\downarrow}(\mathbf{r}), c_{\uparrow}^{\dagger}(\mathbf{r}), -c_{\downarrow}^{\dagger}(\mathbf{r})]$. Note that the anisotropy of Fermi velocities $v_{x,y,z}$ cannot affect qualitatively the Majorana modes bounded to vortex lines, we can simply take that $|v_x| = |v_y| = |v_z| = v_f$ to facilitate the discussion [48]. For this we further absorb the Fermi velocities into the spatial derivative operator by taking $-iv_j \sigma_j \partial_j \rightarrow -i\sigma_j \partial_j$, which can be easily restored later. The vortex line is located at the origin in the (x, y) -plane along the z -axis, hence the choice of cylindrical coordinate (ρ, ϕ, z) . Here $\bar{\Delta}$ is a function that $\bar{\Delta}(\rho \rightarrow 0) = 0$ and $\bar{\Delta}(\rho \rightarrow \infty) = \text{constant}$ and $n\phi$ is the phase winding of the PDW component. H_{eff} can be solved in several steps. First, we perform a spin rotation $U = \exp(-i\frac{\pi}{4}\sigma_z)$ such that

$$U^{-1} \sum_j \sigma_j \partial_j U = \partial_x \sigma_y - \partial_y \sigma_x + \partial_z \sigma_z. \quad (\text{S8})$$

Secondly, we solve $U^{-1} H_{\text{eff}} U$ for a special case $k_z = 0$ (i.e. ignore the $-i\partial_z \sigma_z \tau_z$ term). The details can be found in [48]. The Majorana wave function is $U^{-1} \langle \rho, \phi | \gamma_0 \rangle$. We then perform the inverse spin rotation to obtain the solution for our hamiltonian H_{eff} , the wave function is

$$\langle \rho, \phi | \gamma_0 \rangle = [\tilde{\xi}_1(\rho, \phi), \tilde{\xi}_2(\rho, \phi), \tilde{\xi}_2^*(\rho, \phi), -\tilde{\xi}_1^*(\rho, \phi)]^T,$$

with ($u_0 \equiv \exp[-\int_0^\rho d\rho' \Delta(\rho')]$)

$$\begin{aligned} \tilde{\xi}_1(\rho, \phi) &= e^{i\pi/4} e^{im\phi} u_0(\rho) J_m(\mu_{\text{eff}}\rho), \\ \tilde{\xi}_2(\rho, \phi) &= e^{i3\pi/4} e^{i(m+1)\phi} u_0(\rho) J_{m+1}(\mu_{\text{eff}}\rho), \end{aligned}$$

and the Majorana operator for $k_z = 0$ and $E = 0$ as

$$\hat{\gamma}_0 = \int d^2\mathbf{r} u_0(\rho) \left[e^{i\pi/4} e^{im\phi} J_m(\mu_{\text{eff}}\rho) c_{\uparrow}(\rho, \phi) + e^{i3\pi/4} e^{i(m+1)\phi} J_{m+1}(\mu_{\text{eff}}\rho) c_{\downarrow}(\rho, \phi) + \text{h.c.} \right]. \quad (\text{S9})$$

Note that we have the real condition for Majorana fermions in real space $\gamma^{\dagger} = \gamma$. Here the vortex winding $n \in \mathbb{Z}$ is related to $m \in \mathbb{Z}$ by

$$n = 2m + 1. \quad (\text{S10})$$

Note that only odd vortex windings permit zero-energy solutions at $k_z = 0$. Finally, we add back the $-i\partial_z\sigma_z\tau_z$ term. It is easy to see that the wave function for the Majorana modes have the form

$$\begin{aligned} \langle \rho, \phi, k_z | \gamma_z \rangle &= \exp(ik_z z \sigma_z \tau_z) [\tilde{\xi}_1(\rho, \phi), \tilde{\xi}_2(\rho, \phi), \tilde{\xi}_2^*(\rho, \phi), -\tilde{\xi}_1^*(\rho, \phi)]^T \\ &= [e^{ik_z z} \tilde{\xi}_1(\rho, \phi), e^{-ik_z z} \tilde{\xi}_2(\rho, \phi), e^{-ik_z z} \tilde{\xi}_2^*(\rho, \phi), -e^{ik_z z} \tilde{\xi}_1^*(\rho, \phi)]^T \end{aligned} \quad (\text{S11})$$

and the corresponding energy $E_{\mathbf{k}}$ is given by the eigen-equation (restore the anisotropic Fermi velocities v_j)

$$H_{\text{eff}}\gamma_z = E_{\mathbf{k}}\gamma_z, \quad E_{\mathbf{k}} = \chi_{M\ell}v_z k_z, \quad (\text{S12})$$

where the chirality of the Majorana line mode is $\chi_{M\ell} = +1$. Finally, we have the Majorana operator for $k_z \neq 0$:

$$\begin{aligned} \hat{\gamma}_z(k_z) &= \int d^2\mathbf{r} \gamma_z(\rho, \phi, k_z) \hat{f}(\rho, \phi, k_z) \\ &= \int d^2\mathbf{r} u_0(\rho) \left[+e^{ik_z z} \left(e^{i\pi/4} e^{im\phi} J_m(\mu_{\text{eff}}\rho) c_{\uparrow}(\rho, \phi, z) + \text{h.c.} \right) \right. \\ &\quad \left. + e^{-ik_z z} \left(e^{i3\pi/4} e^{i(m+1)\phi} J_{m+1}(\mu_{\text{eff}}\rho) c_{\downarrow}(\rho, \phi, z) + \text{h.c.} \right) \right], \end{aligned} \quad (\text{S13})$$

which satisfies $\gamma_z(k_z) = \gamma_z^\dagger(-k_z)$ for (real) Majorana fermion.

We note that in the above derivative the condition $n = 2m + 1$ is needed only for the existence of Majorana zero mode at $k_z = 0$. This condition is however not necessary for the existence of Majorana chiral modes along the vortex line. With the chiral properties of Majorana modes the above solution can be generalized to the case with a generic winding number $n = \mathcal{N}$. Actually, such a vortex line is topologically equivalent to $|\mathcal{N}|$ vortex lines with unity winding $n = \text{sgn}(\mathcal{N})$. In the later case each vortex line hosts a branch of chiral Majorana modes. Due to the chiral property putting the n branches of vortex modes together cannot annihilate them, yielding n chiral Majorana vortex modes.

The chirality of the Majorana vortex modes depends on a couple basic properties. First, we consider a Weyl node with opposite chirality χ without sign change in μ_{eff} , which is associated with the case of an inversion symmetric Weyl metal for $\varphi_0 = 0$. Here the transformation is given by that of the particle-hole symmetry \mathcal{C} is the operator for particle-hole symmetry such that $\mathcal{C}H_{\text{eff}}(\mathbf{k})\mathcal{C}^{-1} = H_{\text{eff}}(-\mathbf{k})$. Then we can readily show that a superconducting Weyl node of opposite chirality [the hamiltonian is given by $H_{\text{eff}}(-\mathbf{k})$] has eigenvalues $E = -v_z k_z$ for the corresponding eigenvectors $\mathcal{C}\gamma_z$, or simply $H_{\text{eff}}(-\mathbf{k})\mathcal{C}\gamma_z = (-k_z)\mathcal{C}\gamma_z$. (ii) Next we consider a Weyl node with opposite chirality χ with sign change in μ_{eff} , which is associated with the case of an inversion symmetry broken Weyl metal for $\varphi_0 \neq 0$ and $\mu = 0$. The corresponding transformation is $\mathcal{P} = \tau_z$ such that $\mathcal{P}H_{\text{eff}}(\mathbf{k}, \mu_{\text{eff}})\mathcal{P}^{-1} = -H_{\text{eff}}(-\mathbf{k}, -\mu_{\text{eff}})$. (iii) Finally, we consider flipping the vortex winding $n \rightarrow -n$. The corresponding transformation is $U_1 = i\tau_y$ such that $U_1 H_{\text{eff}}(\mathbf{k}, n = 1)U_1^{-1} = H_{\text{eff}}(\mathbf{k}, n = -1)$. Collecting all these results together, and restoring the anisotropic Fermi velocities \mathbf{v} , that is $H_{\text{eff}}(\mathbf{k}) \rightarrow H_{\text{eff}}(\mathbf{v} \cdot \mathbf{k})$, we thus have

$$\chi_{M\ell} = \text{sgn}(nv_x v_y v_z). \quad (\text{S14})$$

III. Chiral Majorana vortex modes from real-space calculation

For a full real-space diagonalization of the vortex line modes, we consider a vortex line ($n = 1$) and anti-vortex line ($n = -1$) along z -axis, separated from each other in x - y plane, and attached to one of $\Delta_{0,\pm 2Q}$. Note that in considering a vortex and anti-vortex line pair for the system, we can still apply the periodic boundary condition for the numerical calculation. Nevertheless, the momentum \mathbf{k} is no longer good quantum number, and so the Hamiltonian H_{MF} should be diagonalized in real space $\mathbf{r} = (x, y, z)$. The retarded Green's function can be obtained by

$$\hat{G}^R(E) = |\alpha_1\rangle [\hat{G}^R(E)]_{\alpha_1\alpha_2} \langle \alpha_2|, \quad (\text{S15})$$

with basis in the position and spin space $\alpha \equiv (\mathbf{r}, s)$ and $s = \{\uparrow, \downarrow\}$. The elements read

$$[\hat{G}^R(E)]_{\alpha_1\alpha_2} = \sum_{\eta} \frac{U_{\alpha_1\eta} U_{\alpha_2\eta}^*}{E - E_{\eta} + i0^+}. \quad (\text{S16})$$

Here E_{η} and $U_{\alpha\eta}$ are the eigen-energies and corresponding eigenvector matrix obtained after solving the real space Bogoliubov-de Gennes equation for (S1). Then the spin-dependent local spectral functions are given by

$$A_s(x, y, k_z, E) = -\frac{1}{\pi} \text{Im} \langle x, y, k_z, s | \hat{G}^R(E) | x, y, k_z, s \rangle, \quad (\text{S17})$$

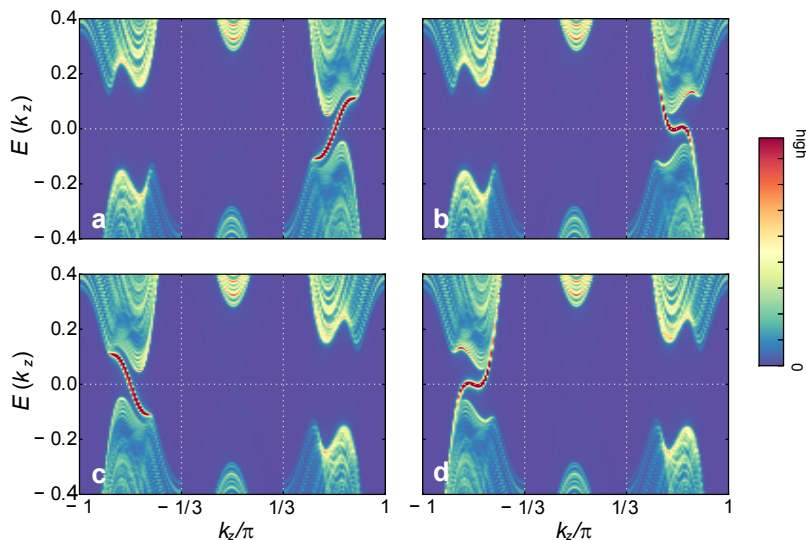


FIG. S1: Local spectral densities $A(k_z, E)$ and chiral Majorana line modes in inversion symmetric Weyl metal. (a) The vortex line with positive winding number $n = +1$ and attached to Δ_{+2Q} ; (b) The vortex line with negative winding number $n = -1$ and attached to Δ_{+2Q} ; (c) The vortex line with positive winding number $n = +1$ and attached to Δ_{-2Q} ; (d) The vortex line with negative winding number $n = -1$ and attached to Δ_{-2Q} . The parameters are that $Q = 2\pi/3$, $\mu = 0.7$, $U = 5.8$, with which the self consistent mean field solutions give $\Delta_0 = -1.849 \times 10^{-2}$ and $\Delta_{\pm 2Q} = 0.2014$. System is periodic in x - and y -axis, while open in z -axis, and has size $N_x/2 = N_y = 55$ and $N_z = 162$.

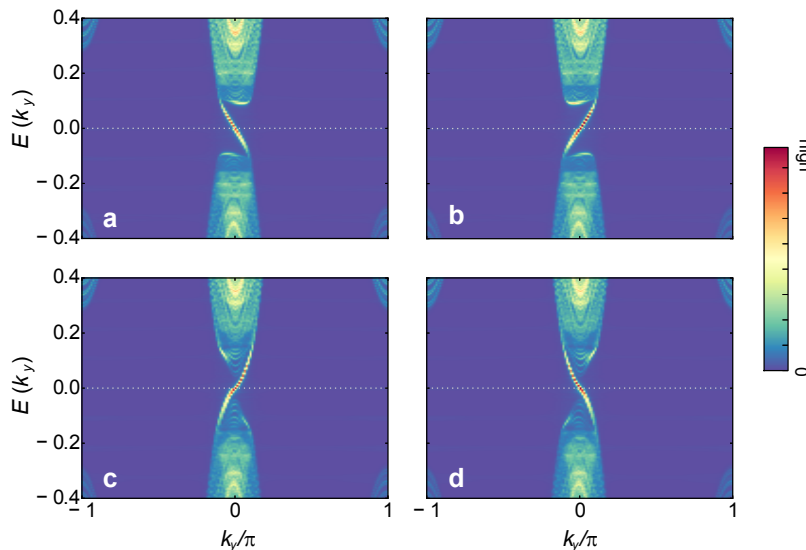


FIG. S2: Numerical results for the configurations similar to those in Fig. S1, except that the vortex lines are along y -axis. The system is also periodic in x - and z -axis, while open in y -axis, and has size $N_x/2 = N_z = 54$ and $N_y = 162$. Besides the chiral Majorana modes, the non-chiral Andreev bound modes are also explicitly obtained in the vortex lines.

where $|x, y, k_z, s\rangle = \frac{1}{\sqrt{N_z}} \sum_z e^{ik_z z} |\mathbf{r}, s\rangle$. We emphasize that due to the PDW order, the momentum k_z of the unfolded BZ is actually not a quantum number either. Nevertheless, to reveal the dispersion of the Majorana modes in the vortex line, we still extract the information of relation between the energy of vortex modes and quantum momentum k_z . Finally, the local spectral function is

$$A(x, y, k_z, E) = \sum_s A_s(x, y, k_z, E). \quad (\text{S18})$$

Computing $A(k_z, E)$ near the vortex core gives the energy spectra of the bulk and the corresponding vortex lines.

Fig. S1(a-d) show the spectra for different configurations. It is clear that in both cases the chiral Majorana vortex modes traverse the bulk gap connecting the lower and upper bands. The chirality of these modes depends on the vortex line winding number and also which pairing order the vortex line is attached to, consistent with the previous analytic solution. As a comparison, we have also done a similar measurement $A(k_y, E)$ for the vortex lines along y -axis and the sign flip property of $\chi_{M\ell}$ remains intact. The results are shown in Fig. S2. These results show that the chiral Majorana line modes observed in the Weyl system is irrespective of the directions.

IV. Emergence of the second Chern number

The second Chern number is defined in the 4D space, while the present physical system is a 3D system. To have a second Chern number, we parameterize the Hamiltonian by taking into account a phase factor of the SC order as $\Delta_{\mathbf{q}} e^{in\theta}$, where $\theta \in [0, 2\pi)$ forms a 1D periodic parameter space S^1 . Together with the 3D lattice, we construct a 4D synthetic space $T^4 = T^3 \times S^1$ spanned by $\mathbf{p} = (\mathbf{p}, p_\theta)$ with $\mathbf{p} = (p_x, p_y, p_z)$ and $p_\theta = \theta$. Let the eigenvectors after solving the mean field Hamiltonian $H_{\text{MF}}(\mathbf{p})$ are $|\alpha, \mathbf{p}\rangle$ (α as band index), we can then compute C_2 by

$$C_2 = \frac{1}{32\pi^2} \int_{T^4} d^4\mathbf{p} \epsilon_{ijkl} \text{Tr}[\mathbf{F}_{ij}\mathbf{F}_{kl}], \quad (\text{S19})$$

where ϵ is the antisymmetric tensor and the gauge field strengths \mathbf{F}_{ij} are calculated based on the non-Abelian gauge potentials \mathbf{a}_j by

$$\begin{aligned} \mathbf{a}_i^{\alpha\beta}(\mathbf{p}) &= -i\langle\alpha, \mathbf{p}|\partial_i|\beta, \mathbf{p}\rangle, \\ \mathbf{F}_{ij}^{\alpha\beta}(\mathbf{p}) &= \partial_i\mathbf{a}_j^{\alpha\beta} - \partial_j\mathbf{a}_i^{\alpha\beta} + i[\mathbf{a}_i, \mathbf{a}_j]^{\alpha\beta}. \\ &= -i(\partial_i\langle\alpha, \mathbf{p}|P_E(\mathbf{p})\partial_j|\beta, \mathbf{p}\rangle - (i \leftrightarrow j)). \end{aligned}$$

Since the Chern numbers are topological invariants, they are not changed as long as the bulk gap of the system is not closed. In this way, the calculation of the Chern numbers can be simplified by deforming the original bulk Hamiltonian so that the bulk bands become flat while keeping the gap to be open. In other words, we consider the diagonalized Hamiltonian in the flat-band limit, given by

$$h_F(\mathbf{p}) = \varepsilon_G P_G(\mathbf{p}) + \varepsilon_E P_E(\mathbf{p}),$$

where $\varepsilon_G < 0$, $\varepsilon_E > 0$ and $P_{G(E)}$ is a projection operator to the occupied (empty) states. With the projection operator the second Chern number can be further calculated by [46]

$$C_2 = \frac{1}{8\pi^2} \int_{T^4} d^4\mathbf{p} \epsilon_{ijkl} \text{Tr}[P_E \partial_i P_G \partial_j P_G P_E \partial_k P_G \partial_l P_G], \quad (\text{S20})$$

where $\partial_i \equiv \frac{\partial}{\partial p_i}$. We note that this expression is gauge invariant and it is suitable for numerical calculation. Numerically, the derivatives are taken using the symmetric difference quotient method, namely

$$\partial_j P_{G,E}(\mathbf{p}_i) = \frac{1}{2\delta_j} [P_{G,E}(\mathbf{p}_i + \delta_j) - P_{G,E}(\mathbf{p}_i - \delta_j)],$$

where individual $\mathbf{p}_i = 2\pi \frac{n_i}{N_i}$ for $n_i = 0, 1, \dots, N_i - 1$, and $\delta_j = \frac{1}{r'} \frac{2\pi}{N_j}$. Here N_i is the discretization in the i -th direction and r' is a parameter added to enhance the accuracy of the derivatives.

On the other hand, if we compute the 2nd Chern number (S19) for only a single superconducting Weyl cone with vortex line based on the low-energy effective Hamiltonian H_{eff} , as given in (S7), we can show that the corresponding second Chern number takes a simple form

$$C_2 = -\chi n \in \mathbb{Z}. \quad (\text{S21})$$

This result is consistent with the 2nd Chern number computed numerically with formula (S20) and based on the full lattice Hamiltonian, as summarized in Table I. We also find that when the system size increases, the magnitude of $|C_2|$ approaches unity. The sign flip property of C_2 is shown in Table II.

U	C_2	Note
5.6	-0.89783698	gapless spectrum
5.7	-0.9554145	Fully gapped
5.8	-0.95628694	Fully gapped
5.9	-0.95659966	Fully gapped
6	-0.9561468	Fully gapped

TABLE I: Second Chern numbers for positive vortex winding $n = +1$ attached to Δ_{+2Q} . We consider inversion symmetric Weyl metal with $\mu = 0.7$ and various U 's. The system size is $N_{x,y,z,\theta} = N_0 = 100$ and derivative enhancing parameter is $r' = 5$.

Vortex lines attached to	Vortex line winding n	C_2
Δ_{+2Q}	+1	-0.95628694
Δ_{+2Q}	-1	+0.95628694
Δ_{-2Q}	+1	+0.95628694
Δ_{-2Q}	-1	-0.95628694

TABLE II: The 2nd Chern number C_2 with respect to χ and n . We consider inversion symmetric Weyl metal with $\mu = 0.7$ and $U = 5.8$. The system size is $N_{x,y,z,\theta} = N_0 = 100$ and derivative enhancing parameter is $r' = 5$.

V. Discussions

We note that in defining the synthetic 4D space, the parameter p_θ for the SC order is a constant variable, independent of real position \mathbf{r} . This definition has nothing to do with the vortex line generated in the real space. On the other hand, once the superconducting Hamiltonian $H_{\text{MF}}(\mathbf{p}, p_\theta)$ for the defined 4D synthetic space is topologically nontrivial, namely, has nonzero 2nd Chern number, it gives rise to novel physical consequences, including that a vortex line generated in the PDW phase hosts chiral Majorana modes.

The emergence of the 2nd Chern number shows that the gapped PDW phase, while being trivial in the 3D, is an intrinsic non-Abelian topological order in the 4D synthetic space. Nevertheless, we note that this emergent topological phase is beyond the ten-fold Altland-Zirnbauer symmetry classification [44]. Actually, within the scope of the current topological classification theory [20–22], the class-D superconductor in 4D should still be topologically trivial, implying that the 4D Hamiltonian $H_{\text{MF}}(\mathbf{p}, p_\theta)$ cannot be characterized by the current topological classification theory. A subtle reason is because the extra dimension, defined through the parameter space p_θ of the SC order, is qualitatively different from the 3D physical space (p_x, p_y, p_z) . This leaves an interesting open question: how to classify the topological states in generic synthetic dimensions.

* Corresponding author: xiongjunliu@pku.edu.cn

- [1] E. Majorana, *Nuovo Cim.* **14**, 171 (2008).
- [2] F. Wilczek, *Nat. Phys.* **5**, 614 (2009).
- [3] J. Alicea, *Reports on Progress in Physics* **75**, 076501 (2012).
- [4] M. Franz, *Nat. Nano.* **8**, 149 (2013).
- [5] N. Read and D. Green, *Phys. Rev. B* **61**, 10267 (2000).
- [6] A. Y. Kitaev, *Physics-Uspekhi* **44**, 131 (2001).
- [7] L. Fu and C. L. Kane, *Phys. Rev. Lett.* **100**, 096407 (2008).
- [8] J. D. Sau, R. M. Lutchyn, S. Tewari, and S. Das Sarma, *Phys. Rev. Lett.* **104**, 040502 (2010).
- [9] R. M. Lutchyn, J. D. Sau, and S. Das Sarma, *Phys. Rev. Lett.* **105**, 077001 (2010).
- [10] Y. Oreg, G. Refael, and F. von Oppen, *Phys. Rev. Lett.* **105**, 177002 (2010).
- [11] S. R. Elliott and M. Franz, *Rev. Mod. Phys.* **87**, 137 (2015).
- [12] V. Mourik, K. Zuo, S. M. Frolov, S. R. Plissard, E. P. A. M. Bakkers, and L. P. Kouwenhoven, *Science (80-.)*. **336**, 1003 (2012).
- [13] M. T. Deng, C. L. Yu, G. Y. Huang, M. Larsson, P. Caroff, and H. Q. Xu, *Nano Lett.* **12**, 6414 (2012).
- [14] A. Das, Y. Ronen, Y. Most, Y. Oreg, M. Heiblum, and H. Shtrikman, *Nat Phys* **8**, 887 (2012).
- [15] S. Nadj-Perge, I. K. Drozdov, J. Li, H. Chen, S. Jeon, J. Seo, A. H. MacDonald, B. A. Bernevig, and A. Yazdani, *Science (80-.)*. **346**, 602 LP (2014).
- [16] J.-P. Xu, M.-X. Wang, Z. L. Liu, J.-F. Ge, X. Yang, C. Liu, Z. A. Xu, D. Guan, C. L. Gao, D. Qian, Y. Liu, Q.-H. Wang,

- F.-C. Zhang, Q.-K. Xue, and J.-F. Jia, Phys. Rev. Lett. **114**, 17001 (2015).
- [17] H.-H. Sun, K.-W. Zhang, L.-H. Hu, C. Li, G.-Y. Wang, H.-Y. Ma, Z.-A. Xu, C.-L. Gao, D.-D. Guan, Y.-Y. Li, C. Liu, D. Qian, Y. Zhou, L. Fu, S.-C. Li, F.-C. Zhang, and J.-F. Jia, Phys. Rev. Lett. **116**, 257003 (2016).
- [18] A. Y. Kitaev, Physics-Uspekhi **44**, 131 (2001).
- [19] X.-L. Qi, T. L. Hughes, S. Raghu, and S.-C. Zhang, Phys. Rev. Lett. **102**, 187001 (2009).
- [20] A. P. Schnyder, S. Ryu, A. Furusaki, and A. W. W. Ludwig, Phys. Rev. B **78**, 195125 (2008).
- [21] A. Kitaev, AIP Conf. Proc. **1134** (2009).
- [22] C.-K. Chiu, J. C. Y. Teo, A. P. Schnyder, and S. Ryu, Rev. Mod. Phys. **88**, 035005 (2016).
- [23] D. A. Ivanov, Phys. Rev. Lett. **86**, 268 (2001).
- [24] J. C. Y. Teo and C. L. Kane, Phys. Rev. B **82**, 115120 (2010).
- [25] P. Fulde and R. A. Ferrell, Phys. Rev. **135**, A550 (1964).
- [26] A. I. Larkin and Y. N. Ovchinnikov, Sov. Phys. JETP **20**, 762 (1965).
- [27] X. Wan, A. M. Turner, A. Vishwanath, and S. Y. Savrasov, Phys. Rev. B **83**, 205101 (2011).
- [28] A. A. Burkov and L. Balents, Phys. Rev. Lett. **107**, 127205 (2011).
- [29] S.-Y. Xu, I. Belopolski, N. Alidoust, M. Neupane, G. Bian, C. Zhang, R. Sankar, G. Chang, Z. Yuan, C.-C. Lee, S.-M. Huang, H. Zheng, J. Ma, D. S. Sanchez, B. Wang, A. Bansil, F. Chou, P. P. Shibayev, H. Lin, S. Jia, and M. Z. Hasan, Science **349**, 613 (2015).
- [30] S.-M. Huang, S.-Y. Xu, I. Belopolski, C.-C. Lee, G. Chang, B. Wang, N. Alidoust, G. Bian, M. Neupane, C. Zhang, S. Jia, A. Bansil, H. Lin, and M. Z. Hasan, Nat. Commun. **6**, 7373 (2015).
- [31] B. Q. Lv, N. Xu, H. M. Weng, J. Z. Ma, P. Richard, X. C. Huang, L. X. Zhao, G. F. Chen, C. E. Matt, F. Bisti, V. N. Strocov, J. Mesot, Z. Fang, X. Dai, T. Qian, M. Shi, and H. Ding, Nat Phys **11**, 724 (2015).
- [32] B. Q. Lv, H. M. Weng, B. B. Fu, X. P. Wang, H. Miao, J. Ma, P. Richard, X. C. Huang, L. X. Zhao, G. F. Chen, Z. Fang, X. Dai, T. Qian, and H. Ding, Phys. Rev. X **5**, 31013 (2015).
- [33] S.-K. Jian, Y.-F. Jiang, and H. Yao, Phys. Rev. Lett. **114**, 237001 (2015).
- [34] A. Kitaev, Ann. Phys. (N. Y.) **303**, 2 (2003).
- [35] C. Nayak, S. H. Simon, A. Stern, M. Freedman, and S. Das Sarma, Rev. Mod. Phys. **80**, 1083 (2008).
- [36] J. Alicea, Y. Oreg, G. Refael, F. von Oppen, and M. P. A. Fisher, Nat Phys **7**, 412 (2011).
- [37] Y.-Q. Wang and X.-J. Liu, Phys. Rev. A **94**, 031603 (2016).
- [38] Z. Wu, L. Zhang, W. Sun, X.-T. Xu, B.-Z. Wang, S.-C. Ji, Y. Deng, S. Chen, X.-J. Liu, and J.-W. Pan, Science **354**, 83 (2016).
- [39] G. Y. Cho, J. H. Bardarson, Y.-M. Lu, and J. E. Moore, Phys. Rev. B **86**, 214514 (2012).
- [40] G. Bednik, A. A. Zyuzin, and A. A. Burkov, Phys. Rev. B **92**, 035153 (2015).
- [41] T. Zhou, Y. Gao, and Z. D. Wang, Phys. Rev. B **93**, 094517 (2016).
- [42] Y. Wang and P. Ye, Phys. Rev. B **94**, 075115 (2016).
- [43] See Supplemental Material [URL] for details on the self-consistent mean field study, analytic results and numerical studies of chiral Majorana modes and the emergent second Chern number [48].
- [44] A. Altland and M. R. Zirnbauer, Phys. Rev. B **55**, 1142 (1997).
- [45] X.-L. Qi, T. L. Hughes, and S.-C. Zhang, Phys. Rev. B **78**, 195424 (2008).
- [46] B. A. Bernevig and T. L. Hughes, *Topological Insulators and Topological Superconductors* (Princeton University Press, 2013).
- [47] C. Wang and M. Levin, Phys. Rev. Lett. **113**, 080403 (2014).
- [48] X.-J. Liu, J. J. He, and K. T. Law, Phys. Rev. B **90**, 235141 (2014).